Inorganic Chemistry

Article

pubs.acs.org/IC

A 3D Oxalate-Based Network as a Precursor for the $CoMn_2O_4$ Spinel: Synthesis and Structural and Magnetic Studies

Jelena Habjanič,[†] Marijana Jurić,*[,†] Jasminka Popović,[†] Krešimir Molčanov,[†] and Damir Pajić[‡]

[†]Ruđer Bošković Institute, Bijenička cesta 54, 10000 Zagreb, Croatia

[‡]Department of Physics, Faculty of Science, University of Zagreb, Bijenička cesta 32, 10000 Zagreb, Croatia

Supporting Information

ABSTRACT: A novel heterometallic oxalate-based compound of the formula $\{[Co(bpy)_3][Mn_2(C_2O_4)_3]\cdot H_2O\}_n$ (**1**; bpy = 2,2′-bipyridine) was synthesized and characterized by elemental analysis, IR spectroscopy, single-crystal X-ray diffraction (XRD), and magnetization measurement. The molecular structure of **1** is made of a three-dimensional (3D) anionic network, $[Mn_2(C_2O_4)_3]_n^{2n-}$, and tris-chelated cations $[Co(bpy)_3]^{2+}$ occupying the vacancies of the framework. Splitting between the zero-field-cooled (ZFC) and field-cooled (FC) branches of susceptibility below the small peak at 13 K indicates magnetic ordering. Compound **1** was used as a single-source precursor for the formation of the mixed-metal oxide $CoMn_2O_4$. This conversion via thermal decomposition was explored by thermal analysis (TGA and DTA), IR spectroscopy, powder XRD, and magnetic susceptibility measurement. From refined structural parameters, it could be seen that the spinel obtained by the thermal treatment of **1** at 800 °C is characterized by the inversion parameter $\delta = 21\%$, and therefore the structural formula at room temperature can be written as $^{tet}[Co_{0.79}Mn_{0.21}]^{oct}[Co_{0.105}Mn_{0.895}]_2O_4$. The temperature dependence of magnetization for $CoMn_2O_4$ points to at least three magnetic phases: the ferrimagnetic state is observed below 83 K, and up to 180 K blocking of the magnetic moments of nanocrystallites of 31 nm appears, transforming to paramagnetic-like behavior above 180 K. Microstructural characterization of the $CoMn_2O_4$ sample was carried out by means of XRD line-broadening analysis.

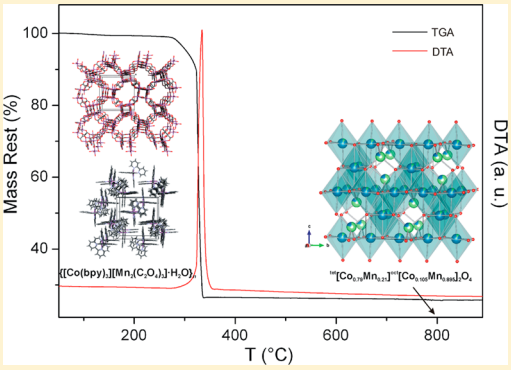

INTRODUCTION

Over the past few decades, there has been a constant growing interest for novel metal−organic frameworks because of their potential applications as functional materials in diverse fields such as hydrogen storage and gas separation, heterogeneous catalysis, luminescence and ion exchange, sensors, or supramolecular magnetism.[1−3]

In the design and synthesis of homo- and heteropolynuclear complexes, as potentially new functional materials with desirable physical properties (mechanical, optical, electrical, or magnetic), an important role belongs to the oxalate ion, $C_2O_4^{2-}$, because of its various possibilities of coordination to metal centers as well as its ability to mediate magnetic interactions between paramagnetic metal ions. So far, a large number of oxalate-based transition-metal species, of different nuclearity and dimensionality, have been synthesized and characterized, with many of them having microporous structure frameworks.[4]

In the search for suitable synthetic routes leading to novel and promising polynuclear species, it has been of considerable importance to find convenient mononuclear complexes that could be used as ligands toward other metal ions. The tris(oxalato)metalate anions $[M(C_2O_4)_3]^{3-}$ (M = trivalent metal) have been widely used as ligands toward metal ions in the preparation of extended multifunctional systems in the last 20 years. The dimensionality and nuclearity of these oxalate-bridged heterobimetallic compounds are controlled by a templating counterion. Therefore, layered two-dimensional (2D) honeycomb structures with the formula cat-$[M^{II}M^{III}(C_2O_4)_3]$ (cat$^+$ = univalent cation) are obtained using $[XR_4]^+$ (X = N and P; R = aryl and alkyl)[5−9] or even the decamethylmetallocenium unit $[A(Cp^*)_2]^+$ (A = Fe and Co; Cp* = pentamethylcyclopentadienyl) as a cation,[10,11] whereas the tris-chelated $[M(bpy)_3]^{2+}$ or $[M(bpy)_3]^{3+}$ (bpy = 2,2′-bipyridine) entities provide chiral anionic three-dimensional (3D) networks of the formulas $[M^{II}_2(C_2O_4)_3]^{2-}$,[8a,12,13] $[M^{I}M^{III}(C_2O_4)_3]^{2-}$,[8a,12b,13b,14] and $[M^{II}M^{III}(C_2O_4)_3]^{-}$.[15] All of these and other similar 2D and 3D systems[16] are examples of multifunctional molecular-based materials in which the magnetic properties are often complemented by additional properties such as electrical conductivity,[11c,16c] prefixed chirality,[8b,10,15a,16b,c] and nonlinear optical activity.[9] Also, the use of the $[Cr(C_2O_4)_3]^{3-}$ unit yielded heterometallic one-dimensional (1D) chains.[17]

The possibility of using coordination polymers (through the thermal decomposition process) as molecular precursors in the synthesis of nanomaterials with high surface and specific

Received: May 15, 2014
Published: August 25, 2014

   dx.doi.org/10.1021/ic501134y | *Inorg. Chem.* 2014, 53, 9633−9643

morphology has been considered only recently.[18−22] This method of obtaining oxide materials, compared with conventional methods, has several advantages: (i) the obtained material is more homogeneous because the metals are mixed at the molecular level; (ii) the resulting materials have relatively high specific surface areas because the crystalline oxides are formed under significantly milder conditions than those in, for instance, solid-state reaction processes; (iii) the existence of bridging or chelating ligands in the precursors prevents metal separation during oxide formation; (iv) there is much greater control of the metal stoichiometry in the final oxide.[19]

The $C_2O_4^{2-}$ anion in oxalate-based solids can easily decompose to the vapor phases, CO_2 and CO, by the low-temperature routes and thus could serve as a convenient source of oxides.[23] Because of their low thermal stability, heterometallic oxalate complexes have already been used for the preparation of mixed-metal oxides.[23−30]

As a continuation of our research program concerning the design and synthesis of homo- and heteropolynuclear complexes with the aim of obtaining potentially new functional materials, herein we report the synthesis and structural, spectroscopic, and magnetic properties of new 3D oxalate-bridged compound $\{[Co(bpy)_3][Mn_2(C_2O_4)_3]\cdot H_2O\}_n$ (**1**; bpy = 2,2′-bipyridine). Considering the preparation of the oxide materials via thermal decomposition of metal−organic complexes, compound **1** has served as a single-source precursor for preparation of the oxide $CoMn_2O_4$. As part of this investigation, the structural, spectroscopic, and magnetic properties of this spinel were also carried out.

It is known that the spinel compounds AB_2O_4 (A = Zn, Fe, Co, Ni, Mn, Mg, Cd, etc.; B = Co, Fe, Cr, Al, Ga, Mn, etc.) have attracted a great deal of research interest linked to a wide range of applications including magnetism, electronics, and catalysis, as well as energy storage and conversion, as a result of their diverse properties. Among the numerous varieties of spinels, AMn_2O_4 is one of the most interesting composite oxides because manganese has numerous advantages, including low cost, high abundance, low toxicity, multiple valences, and a prominent Jahn−Teller effect. Manganese-based spinels have a wide range of versatile applications, including lithium insertion electrodes, magnetic materials, and catalysts. Their physicochemical properties are highly sensitive to the composition, structural parameters, and distribution and oxidation state of cations, which depend greatly on the synthesis conditions. The traditional synthesis of spinel compounds is a solid-state route that involves the grinding and firing of a mixture of oxides, nitrates, or carbonates. Solid-state reactions generally require high temperatures or a long-term repeating process to overcome diffusional barriers.[31]

So far, Coronado et al. published the synthesis and magnetic characterization of a new family of 2D oxalate-bridged networks with the general formula $\{[M^{II}(H_2O)_2]_3[M^{III}(C_2O_4)_3]_2(18\text{-crown-}6)_2\}$ (M^{III} = Cr and Fe; M^{II} = Mn, Fe, Co, and Ni; 18-crown-6 = $C_{12}H_{24}O_6$). The controlled thermal decomposition of these soluble molecular precursors generated pure phases of crystalline mixed oxides with spinel-like structures.[32] Also, there are a few reports of thermal decomposition of layered double hydroxide (LDH)-type precursors, which can be made to incorporate a broad range of trivalent and/or divalent metal cations into pure-phase spinels.[33] It is also known that nanocrystalline spinel ferrites can be prepared from LDH−CO_3 by mechanical milling.[34]

Taking into account the preparation of mixed oxide materials via thermal decomposition of well-defined heterometallic complexes, the coordination polymer **1** represents a prospective and applicable precursor for synthesis of the spinel oxide $CoMn_2O_4$.

EXPERIMENTAL SECTION

Materials. The starting species $K_3[Mn(C_2O_4)_3]\cdot 3H_2O$ and $[Co(bpy)_3]X_2\cdot 6H_2O$ (X = Cl^- and NO_3^-) were prepared according to the method described in the literature.[35,36] All other chemicals were purchased from commercial sources and used without further purification.

Physical Measurements. Elemental analyses for C, H, and N were carried out using a PerkinElmer model 2400 microanalytical analyzer. Metal analysis was performed on a JEOL model 7000F high-resolution thermal field scanning electron microscope with an energy-dispersive X-ray spectroscopy (EDS) system for microanalysis (INCA 350 50; Oxford Instruments).

IR spectra were recorded using KBr pellets with a Bruker Alpha Fourier transform infrared spectrometer in the 4000−350 cm^{-1} region.

Thermal measurements were carried out on a Shimadzu DTG-60H analyzer in the range from room temperature (RT) to 1500 °C in a stream of synthetic air, at a heating rate of 10 °C min^{-1}.

Preparation of $\{[Co(bpy)_3][Mn_2(C_2O_4)_3]\cdot H_2O\}_n$ (1). To an aqueous solution (10 mL) of $K_3[Mn(C_2O_4)_3]\cdot 3H_2O$ (0.0490 g, 0.1 mmol) were added dropwise with stirring at RT an aqueous solution (5 mL) of $CoCl_2\cdot 6H_2O$ (0.0240 g, 0.1 mmol) and an ethanol solution (5 mL) of 2,2′-bipyridine (0.0480 g, 0.3 mmol). Immediately, from the resulting clear orange solution, the yellow octahedral crystals of **1** started to appear and the process of crystallization was complete within a period of 3 days. The crystals of **1** were separated from the solution by filtration, washed with water and ethanol, and left to dry in air. The yield was 45% (based on Mn). Anal. Calcd for $C_{36}H_{24}CoMn_2N_6O_{14}$: C, 46.32; H, 2.59; N, 9.00. Found: C, 46.58; H, 2.52; N, 9.15. IR data (KBr): $\tilde{\nu}$ 3426 (w, br), 3101 (w), 3075 (w), 2974 (w), 2931 (w), 1653 (s), 1629 (vs), 1608 (vs), 1488 (m), 1468 (m), 1440 (s), 1360 (m), 1310 (s), 1247 (w), 1225 (w), 1178 (w), 1156 (w), 1100 (w), 1063 (w), 1018 (m), 982 (w), 920 (m), 797 (s), 780 (s), 738 (m), 651 (w), 632 (w), 568 (w), 491 (w), 420 (w).

Single-Crystal X-ray Diffraction (XRD). The X-ray data for single crystals of compound **1** were collected at 293(2) K by ω scans on an Oxford Diffraction Xcalibur Nova R diffractometer using graphite-monochromated Cu Kα radiation (λ = 1.54179 Å, microfocus tube, CCD detector). Because the compound crystallizes in the chiral space group $P4_132/P4_332$, the Friedel pairs were measured in order to unambiguously establish the correct space group and absolute configurations of the octahedral metal centers. Therefore, the correct space group is $P4_132$, the correct absolute configurations of the octahedral metal centers are Λ, and the metal oxalate helices are *P*. Data reduction, including the multiscan absorption correction, was performed with the *CrysAlisPRO* software package.[37] Solution, refinement, and analysis of the structure was performed using the programs integrated in the *WinGX* system.[38] The structure was solved using *SHELXS97*[39] and refined with *SHELXL97*.[39] The model was refined using the full-matrix least-squares refinement; all non-H atoms were refined anisotropically. The H atoms were treated as constrained entities, using the command *AFIX* in *SHELXL97*.[39] Molecular geometry calculations were performed by *PLATON*,[40] and the molecular graphics were prepared using the *ORTEP-3*[41] and *CCDC-Mercury*[42] programs. The crystal data and details of data collection and refinement for the structure reported in this paper are summarized in Table 1.

Crystallographic data for this paper can be obtained free of charge via www.ccdc.cam.ac.uk/conts/retrieving.html (or from the Cambridge Crystallographic Data Centre, 12 Union Road, Cambridge CB2 1EZ, U.K.; fax +44 1223 336033 or e-mail deposit@ccdc.cam.ac.uk). CCDC 996073 contains the supplementary crystallographic data for this paper.

dx.doi.org/10.1021/ic501134y | Inorg. Chem. 2014, 53, 9633−9643

Table 1. Crystallographic Data and Structure Refinement Details for Compound 1

compound	**1**
empirical formula	$C_{36}H_{24}CoMn_2N_6O_{14}$
fw (g mol^{-1})	933.44
cryst dimens (mm^3)	0.11 × 0.11 × 0.06
cryst syst	cubic
space group	$P4_132$
a (Å)	15.6685(1)
Z	4
V (Å^3)	3846.65(4)
D_{calc} (g cm^{-3})	1.612
μ (mm^{-1})	9.270
Θ range (deg)	3.99–75.44
T (K)	293(2)
diffractometer type	Xcalibur Nova
range of h, k, l	$-18 < h < 18$
	$-13 < k < 13$
	$-18 < l < 18$
reflns collected	6299
indep reflns	1305
obsd reflns ($I \geq 2\sigma$)	1253
abs corrn	multiscan
R_{int}	0.0239
$R(F)$	0.0278
$R_w(F^2)$	0.0748
goodness of fit	1.072
H-atom treatment	constrained
no. of param	94
$\Delta\rho_{max}$, $\Delta\rho_{min}$ (e Å^{-3})	0.361, −0.141
Flack parameter	−0.020(5)

Magnetic Study. Magnetization M of all compounds was measured using a MPMS 5 commercial SQUID magnetometer. The temperature dependence of magnetization, $M(T)$, of complex **1** was measured in 10 Oe, 100 Oe, and 1 kOe magnetic fields in the temperature range 2–330 K, and of the oxide $CoMn_2O_4$ in fields of 1 Oe, 10 Oe, 100 Oe, 1 kOe, and 10 kOe in the temperature range 2–360 K. Two modes of measurement were applied: after cooling in zero field (ZFC) and after cooling in a magnetic field (FC), in which measurement is performed during heating. Field dependences of magnetization, $M(H)$, i.e., magnetic hysteresis loops, were measured at several stable temperatures in fields of up to 50 kOe. Measured magnetic moments of the samples were corrected against the sample-holder contribution and temperature-independent contributions of core electrons in accordance to the well-known Pascal constants. The molar magnetic susceptibility $\chi = M/H$ of complex **1** was calculated for measurement in field 100 Oe.

Thermal Synthesis of the Oxide $CoMn_2O_4$. Finely ground crystalline powders of compound **1** were heated in a thermal analyzer to a certain temperature, in the range from RT to 1000 °C, in a stream of synthetic air, at a heating rate of 10 °C min^{-1}. After decomposition, the resulting oxide products were characterized by powder XRD. IR data (KBr) of the $CoMn_2O_4$ phase obtained at 800 °C: $\tilde{\nu}$ = 3447 (w, br), 2925 (sh), 1636 (w), 638 (s), 542 (s), 420 (m), 360 (w).

Powder X-ray Structural Study. Structural characteristics of the powder product obtained by the heat treatment of **1** at 800 °C were studied at RT by powder XRD using a Philips MPD 1880 counter diffractometer with Cu Kα radiation. The sample was scanned in step mode (2θ = 0.02°); data were collected in the range 10–70° with a fixed counting time of 7 s step^{-1}. Rietveld refinement was performed by *X'Pert HighScore Plus*, version 2.1 (PANalytical, 2004), with a pseudo-Voigt function used for describing the profiles. A polynomial function was used as the background model. Size–strain analysis was performed in the course of Rietveld refinement. Crystallite sizes were also calculated for different crystallographic directions by the *XBroad* program,[43] which performs Stokes deconvolution[44] in order to separate instrumental contribution from pure diffraction broadening, followed by Warren–Averbach analysis.[45] Namely, for each diffraction line, *XBroad* calculates the first 20 Fourier coefficients and generates a $F(L)$ versus L plot, where $L = \lambda t/4(\sin\Theta_M - \sin\Theta_0)$ and t is the order of the Fourier coefficient. The initial slope of the $F(L)$ plot when L

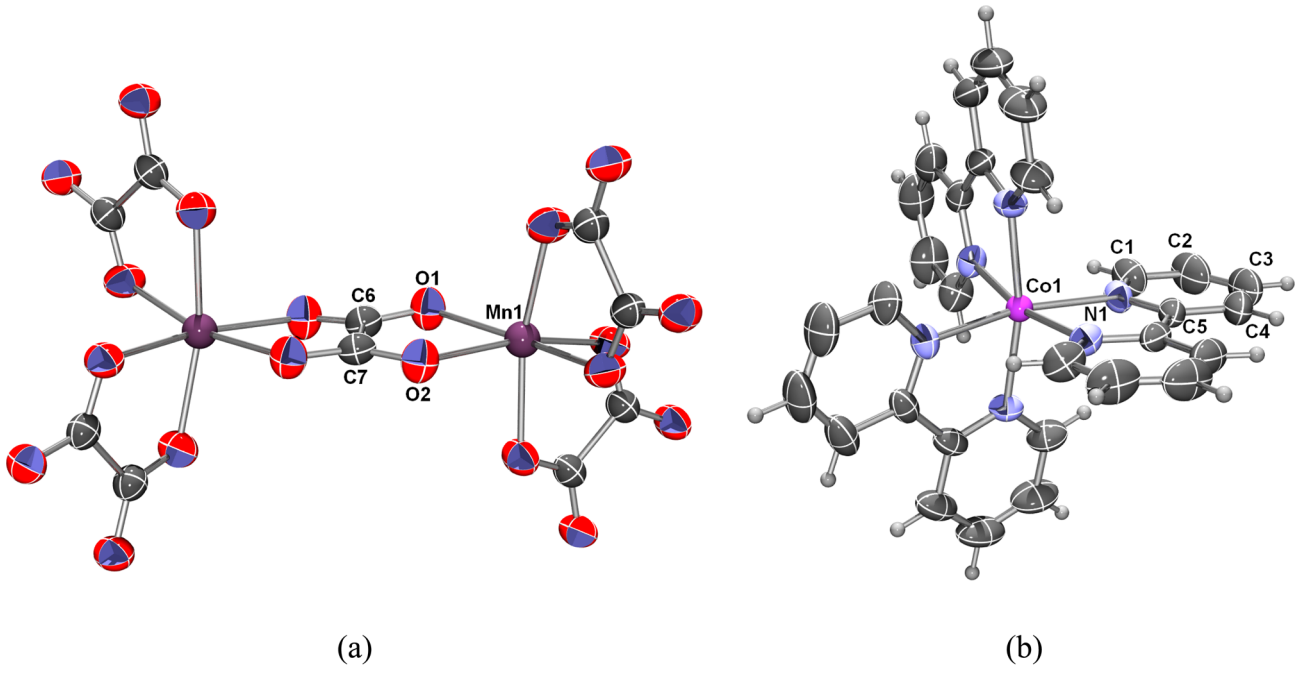

Figure 1. Coordination of the metal centers in the (a) $[Mn_2(C_2O_4)_3]_n^{2n-}$ network and (b) $[Co(bpy)_3]^{2+}$ discrete cation, in compound **1** with atom numbering scheme. Octahedrally coordinated metal atoms have a Λ configuration. Atomic displacement ellipsoids are drawn at the 50% probability level, and the H atoms are depicted as spheres of arbitrary radii. Because of the symmetry requirements of their special positions, the displacement parameters of metal atoms are spherical.

dx.doi.org/10.1021/ic501134y | *Inorg. Chem.* 2014, 53, 9633–9643

approaches zero, $\langle L \rangle = -(1/dF(L)/dL)$, gives a negative reciprocal value of the average column length, i.e., average crystallite size in the direction perpendicular to the lattice planes. Silicon powder was used as the instrumental broadening standard. Molecular graphics were prepared using *VESTA*.[46]

RESULTS AND DISCUSSION

I. Characterization of Compound 1. The title compound was obtained in the form of yellow octahedral crystals from the reaction of aqueous solutions of $K_3[Mn(C_2O_4)_3]\cdot 3H_2O$ and $CoCl_2\cdot 6H_2O$ and an ethanol solution of 2,2′-bipyridine in the molar ratio of 1:1:3. Immediately after mixing initial solutions, a significant color change, from dark red to orange-yellow, is observed. It is known that reduction of Mn^{3+} occurs in slightly acidic solutions.[47] When the same components were taken in 1:1:2 or 1:1:4 ratios, compound **1** resulted in a lower yield and purity. Single crystals of **1** formed also by the slow evaporation of aqueous solutions containing $K_3[Mn(C_2O_4)_3]\cdot 3H_2O$ and $[Co(bpy)_3]X_2\cdot 6H_2O$ (X = Cl^- and NO^{3-}) in the ratios 1:1 or 1:2, but their yields were also rather low.

The compound is moderately air-stable. It is not soluble in water and common organic solvents. EDS analysis on a few single crystals of **1** showed a Co/Mn ratio of 1:2.

Molecular and Crystal Structure of 1. The molecular structure of **1** is made of 3D anionic network $[Mn_2(C_2O_4)_3]_n^{2n-}$, with an uncoordinated water molecule and tris-chelated cations $[Co(bpy)_3]^{2+}$ occupying the vacancies of the framework. The coordination of the metal centers in a network and discrete cation are shown in Figure 1.

Both metal atoms, Co and Mn, are located in special positions: the Co atom at an intersection of one 3-fold and three 2-fold axes (at $^5/_8$, $^7/_8$, $^1/_8$, Wyckoff position a, site symmetry 32, multiplicity 4) and the Mn atom at a 3-fold axis (at $\bar{x} + {}^1/_2$, $\bar{x}$, $x + {}^1/_2$, Wyckoff position c, site symmetry 3, multiplicity 8).

The Mn^{II} and Co^{II} atoms are coordinated by three chelating ligands (oxalate and bipyridine, respectively), displaying an approximately octahedral coordination geometry (Figure 1). Selected bond lengths and angles in compound **1** are given in Table 2. The values of the Mn−O and Co−N bond lengths are in good agreement with the literature data.[4]

Table 2. Geometric Parameters of Metal Coordination Spheres (Å and deg)[a]

Co1−N1	2.1285(16)	N1−Co1−N1^{iv}	167.79(7)
Mn1−O1	2.1642(16)	O1−Mn1−O2^{v}	77.30(5)
Mn1−O2	2.1731(16)	O1−Mn1−O1^{vi}	99.40(6)
N1−Co1−N1^{i}	77.00(7)	O1−Mn1−O2^{vi}	166.92(6)
N1−Co1−N1^{ii}	94.65(7)	O1−Mn1−O2^{vii}	93.64(7)
N1−Co1−N1^{iii}	94.90(7)	O2−Mn1−O2^{vii}	90.20(6)

[a]Symmetry operators: (i) $^1/_4 + x$, $-{}^1/_4 + y$, $^1/_4 - z$; (ii) $-{}^1/_2 + x$, $^3/_2 - y$, $1 - z$; (iii) $^3/_4 - x$, $^7/_4 - y$, $^3/_4 - z$; (iv) $^5/_4 - x$, $-{}^3/_4 + y$, $^3/_4 + z$; (v) $1 - x$, $^1/_2 + y$, $^1/_2 - z$; (vi) $-{}^1/_2 + x$, $^1/_2 - y$, $1 - z$; (vii) $-{}^1/_2 + x$, $^1/_2 - y$, $1 - z$.

The crystal packing of **1** is clathrate-like, with a well-known chiral 3D 3-connected decagon (10,3) oxalate-based anionic network configuration, with the formal $[Mn(C_2O_4)_{3/2}]$ units representing 3-connecting nodes (Figure 2a). The bis(bidentate) oxalate ligands repeatedly bridge adjacent Mn^{2+} ions in all three dimensions, which finally leads to a polymeric net. The $[Co(bpy)_3]^{2+}$ cations are located inside the large decagonal voids of this framework (Figures 2 and 3). The size of the holes of the anionic framework is large enough to encapsulate one guest. The Mn···Mn separation across the oxalate bridge is 5.597(3) Å.

The relative configuration between two adjacent chiral hexacoordinated metal centers determines the dimensionality of the network. A heterochiral arrangement, i.e., (ΔM_1, ΛM_2) or (ΛM_1, ΔM_2), leads to a 2D network; the anionic sublattice displays a honeycomb structure, while the cationic moiety, which usually is $[XR_4]^+$ (X = N and P; R = aryl and alkyl), is located between the anionic layers.[5−9] On the other hand, homochiral arrangement (ΔM_1, ΔM_2) or (ΛM_1, ΛM_2) leads to a 3D network built from a (10,3) anionic network, while the associated cationic counterpart, possessing the same D_3 symmetry as that of the connected metal centers, fits in the vacancies. In the case of 3D networks, the homochiral arrangement of the bimetallic framework displays a helical structure. The right or left twist of the helices depends on the absolute configuration of the connected metal centers, namely, *M* (left-handed) for Δ and *P* (right-handed) for Λ.[15a]

The compound crystallized as a racemic conglomerate, containing enantiomeric crystals belonging to enantiomeric space groups $P4_132$ and $P4_332$. In our structure, an absolute configuration was established in the $P4_132$ space group. The Mn atom is chelated by the oxalate ligands in the Λ configuration, leading to anionic helices of configuration *P*. The Co atom from the tris-chelated cation also has the Λ configuration. Therefore, in $P4_332$, the octahedral atoms are Δ, while the metal oxalate helices are *M*.

Compound **1** is a dihydrate, with two disordered water molecules occupying the center of the hydrophobic cavity formed by three adjacent $[Co(bpy)_3]^{2+}$ cations (Figure 4). Because the void is relatively large and the cations have neither proton donors nor acceptors, the water is disordered about a 3-fold axis. It is modeled as an O atom located at $\bar{y} + {}^1/_4$, $^7/_8$, $y + {}^1/_2$ (Wyckoff position d, site symmetry 2, multiplicity 12).

Only electrostatic interactions as well as weak C−H(bpy)···O hydrogen bonds exist between the cation and anion network (with the proton acceptors being the oxalate O atoms); however, no close contacts between cations are observed.

IR Study of Compound 1. In the IR spectrum of compound **1**, absorption bands that can be attributed to the vibrations of the bis(bidentate) bridging oxalate groups, coordinated 2,2′-bipyridine ligands, and water molecules are present. The broad band of weak intensity with a maximum of around 3426 cm^{-1} is in agreement with the presence of water molecules. The absorption bands corresponding to the bridging oxalate ligand are located at 1653 and 1629 cm^{-1} [ν_{as}(CO)], 1360 and 1310 cm^{-1} [ν_s(CO)], and 797 cm^{-1} [δ(OCO)]. Other absorption bands in the spectra originate from different vibrations of coordinated 2,2′-bipyridine molecules.[48]

Thermal Analysis of Compound 1. The thermal behavior of the title compound has been studied by simultaneous thermogravimetric analysis (TGA) and differential thermal analysis (DTA) performed on a crystalline sample in a stream of synthetic air, up to 1000 °C (Figure 5). The TGA curve shows single-step decomposition with a mass loss of 74.03% (calcd 74.17%), which takes place in a narrow temperature range, 260−380 °C. This step could be associated with the removal of three molecules of the bipyridine, together with elimination of the oxalate groups ($3CO + 3CO_2$). The accompanying DTA curve shows the exothermic effect, with a maximum at 333 °C. Afterward, the remaining mass stays

dx.doi.org/10.1021/ic501134y | Inorg. Chem. 2014, 53, 9633−9643

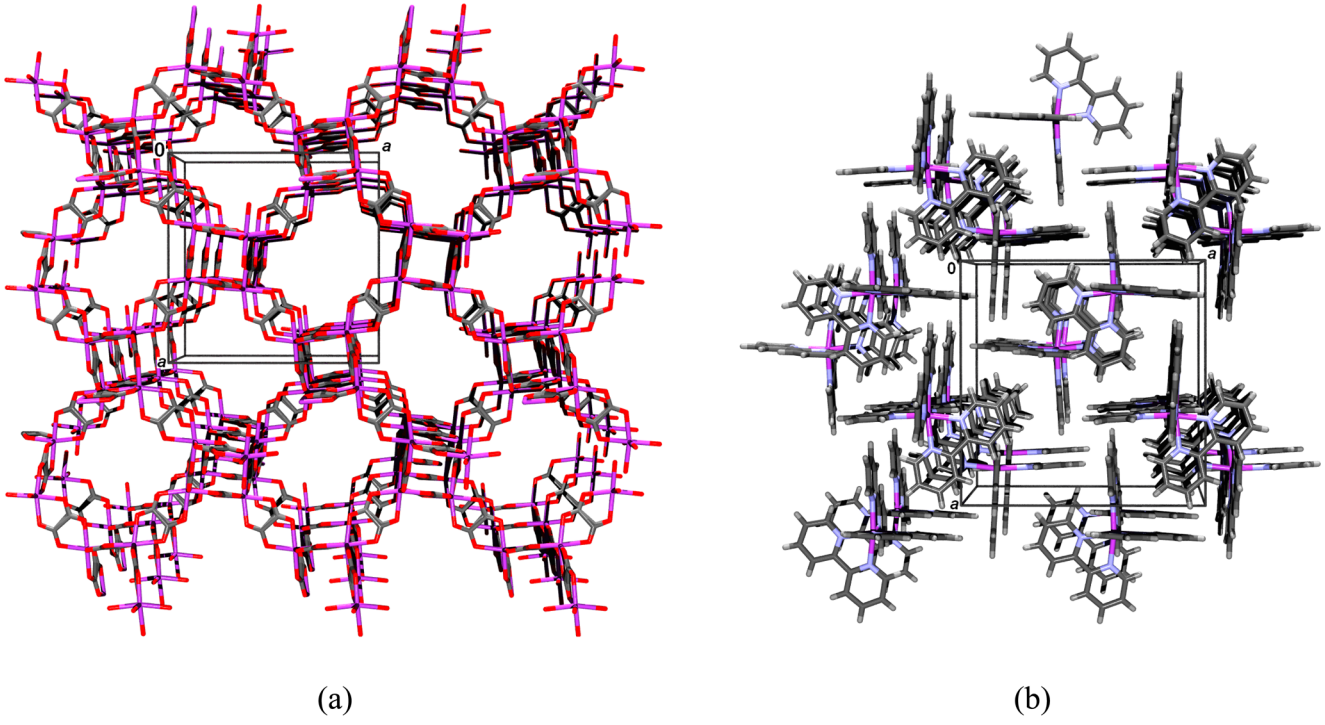

Figure 2. Crystal packing in compound **1** of (a) a 3D (10,3) oxalate-based anionic $[Mn_2(C_2O_4)_3]_n^{2n-}$ network, leading to anionic helices of configuration *P*, and (b) $[Co(bpy)_3]^{2+}$ cations, which occupy decagonal voids in the anionic network.

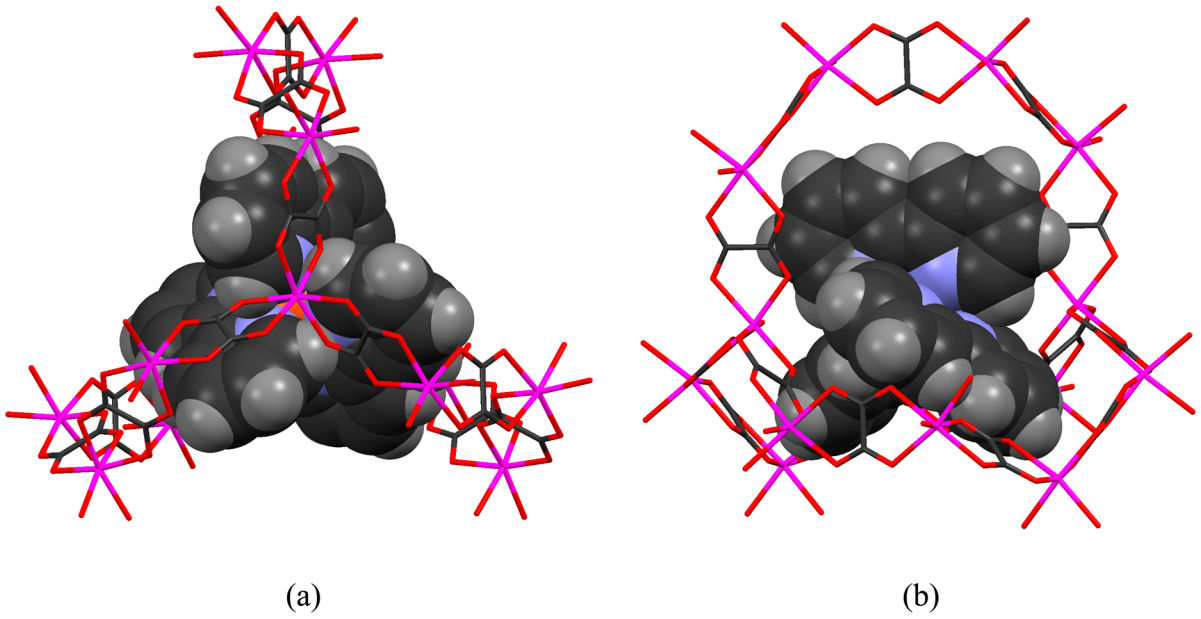

Figure 3. Decagon of a $[Mn_2(C_2O_4)_3]_n^{2n-}$ network wrapped around a $[Co(bpy)_3]^{2+}$ cation in compound **1** viewed (a) in the direction [111] (i.e., along a 3-fold axis) and (b) approximately perpendicular to the 3-fold axis.

constant, with the black final residue corresponding to the $CoMn_2O_4$ oxide (exp 25.68%; calcd 25.32%). No further changes on the TGA and DTA curves were observed from 400 to 1000 °C, suggesting that the phase composition of the residues in the selected range remained unchanged. The residue obtained after thermolysis of **1** at selected temperature was studied by powder XRD.

Magnetization Study. The temperature dependence of magnetization *M* measured in several magnetic fields (10, 100, and 1000 Oe) and susceptibility χ calculated from the 100 Oe field of compound **1** are shown in Figure 6. At first glance, the temperature dependence of susceptibility is paramagnetic.

In almost a paramagnetic behavior of $\chi(T)$, a small kink near 15 K is observed. Additional measurements connected this small anomaly with the transition to some ordered magnetic state. A clearly visible splitting between the zero-field-cooled (ZFC) and field-cooled (FC) branches of susceptibility (inset of Figure 6) is still more pronounced in measurement with a much smaller field below 13 K, while for a field of 1 kOe, the ZFC−FC splitting diminishes. This phenomenon is usually

dx.doi.org/10.1021/ic501134y | *Inorg. Chem.* 2014, 53, 9633−9643

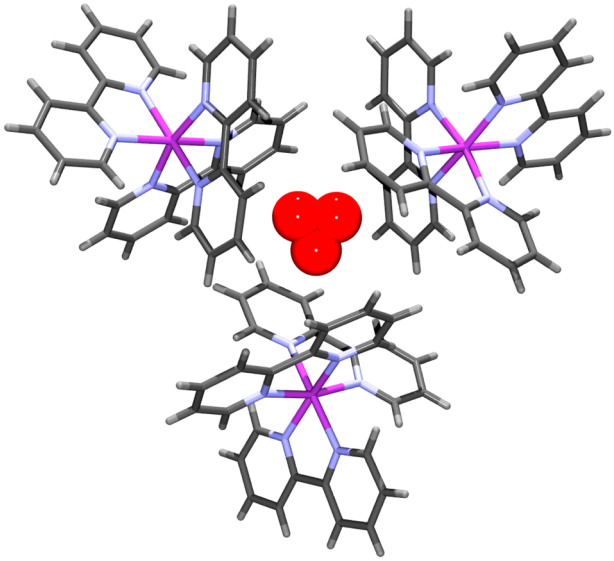

Figure 4. Hydrophobic cavity formed by three $[Co(bpy)_3]^{2+}$ cations containing disordered water molecules, viewed approximately in the direction of the 3-fold axis. O atoms are arbitrarily scaled.

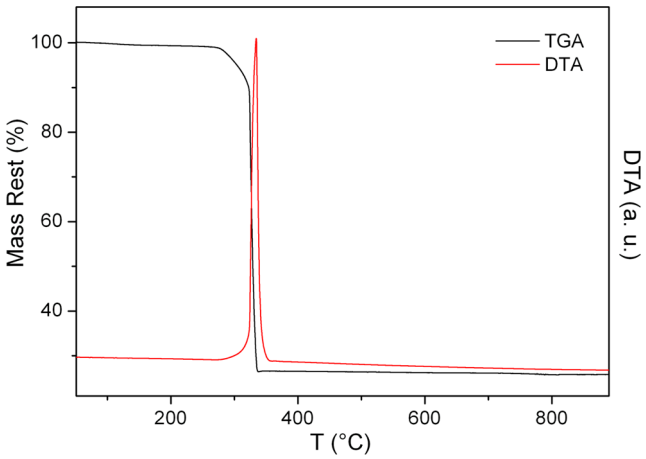

Figure 5. TGA and DTA curves for compound **1** measured in synthetic air.

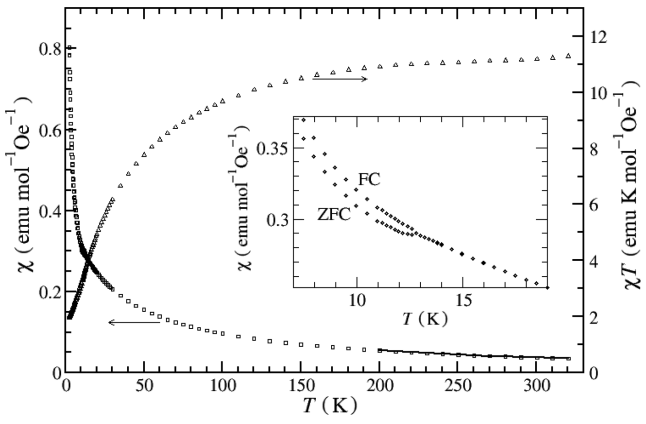

Figure 6. Temperature dependence of magnetic susceptibility (squares, left axis) and χT product (triangles, right axis) of compound **1**. The line for T above 200 K is the Curie–Weiss fitting curve. Inset: susceptibility enlarged near the anomaly.

connected with short- or long-range ordering, spin glass, or another kind of more complex local order. On the basis of the structure of compound **1**, we could conclude that a magnetic-ordered phase appears across the Mn framework, along with the superposition of independent Co paramagnetism.

Near RT, the susceptibility is in agreement with the high-spin states of both ions ($^5/_2$ for Mn^{2+} and $^3/_2$ for Co^{2+}) and the g factors already observed in similar geometries (1.95 for Mn^{2+} and 2.55 for Co^{2+}).[49] Our value χT of 11.3 emu mol^{-1} K, as well as Curie's constant, is in agreement with the observed 11.4 emu mol^{-1} K per $CoMn_2$ unit.[22] A slightly higher value than the spin only (10.6 emu mol^{-1} K) is attributed to the orbital contribution coming from Co^{2+} in octahedral coordination. Comparing the shape of $\chi T(T)$ with thorough studies of the influence of orbital contributions and spin–orbit coupling on the susceptibility,[50,51] we could conclude that the orbital reduction factor as well as the ligand-field splitting of the orbital degeneracy is relatively small.

The separation of each contribution, namely, the magnetic responses of Mn framework and Co paramagnetism, is not obvious because the Mn^{2+} ions show considerable zero-field splitting in octahedral coordination at temperatures near and below the phase transition and Co^{2+} ions exhibit considerable orbital contributions and spin–orbit coupling that affect the whole temperature range.[50,51] More quantitative description would require additional theoretical modeling, which is beyond the scope of this work.

At high enough temperatures (above 200 K), where the Co^{2+}-related orbital peculiarities cease, the Weiss parameter of −3.0 K is reliably obtained, pointing to the antiferromagnetic interactions that lead to the long-range magnetic transition observed at 13 K. Hysteresis loops $M(H)$ showed no measurable irreversibility even below the magnetic transition temperature, putting the coercive field below the amount of remnant field in the superconducting magnet of the instrument (up to 4–5 Oe). This could indicate that the order is not typically ferromagnetic but originates from antiferromagnetic exchange over the oxalate bridges. Moreover, the maximal measured magnetization (at the lowest temperature of 2 K and in the highest field of 50 kOe) is 22 emu g^{-1}, corresponding to 4.3 Bohr magnetons (μ_B) per formula unit. This is considerably lower than the value expected in the case of the ferromagnetic order (around 13 μ_B) of observed spins but slightly above the Co^{2+} paramagnetic contributions. $M(H)$ is still far from saturation, being reminiscent of the antiferromagnetic curve. Therefore, we can make conclusions about the antiferromagnetic network of Mn^{2+} spins, where the magnetic field produces their canting. Above transition temperature, $M(H)$ is linear, in accordance with the susceptibility shown in Figure 6.

Magnetic order is confirmed below 13 K, where the temperature hysteresis appears, and neither zero-field splitting nor orbital and spin–orbit contributions could produce such a kink. However, the superposition of many nontrivial terms makes it hard to describe the magnetic ground state in an ordered framework, except to say that it is an antiferromagnetic network of slightly canted Mn^{2+} spins with incorporated paramagnetic Co^{2+} contributions.

II. Characterization of the Mixed Oxide $CoMn_2O_4$. It is well-known that $CoMn_2O_4$ crystallizes in a hausmannite-type structure, which can be described as a Jahn–Teller distortion of the spinel structure due to the presence of Mn^{3+} in the octahedral site. The spinel structure AB_2O_4 generally consists of a closely packed array of O^{2-}, with A^{2+} cations residing on the

dx.doi.org/10.1021/ic501134y | Inorg. Chem. 2014, 53, 9633–9643

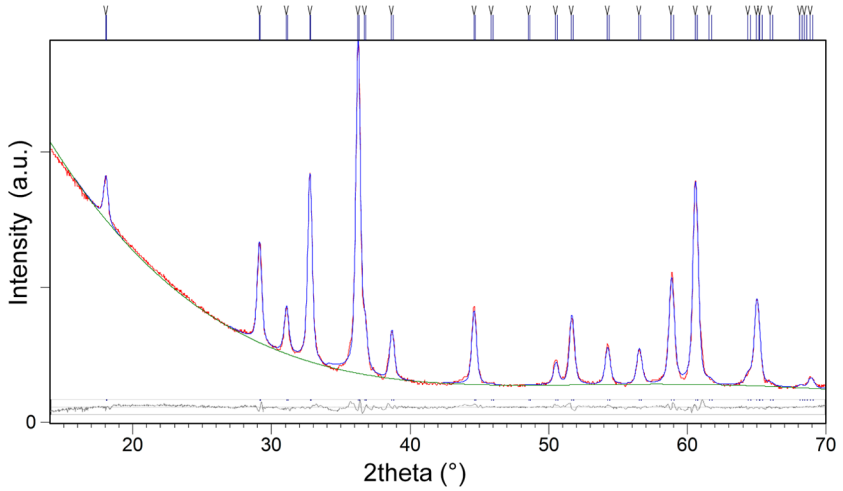

Figure 7. Graphical result of the final Rietveld refinement of RT data for the $CoMn_2O_4$ phase, obtained by heating compound **1** at 800 °C followed by cooling to RT. The blue vertical marks represent the positions of the $CoMn_2O_4$ phase. Experimental data are shown in blue, the calculated pattern is in red, and the difference curve is in gray.

tetrahedral site and B^{3+} ions on the octahedral site. However, spinels are known to exhibit some degree of disorder, defined by the inversion parameter δ. The inversion parameter is defined as a fraction of the divalent cations residing on the octahedral site. Some of the principal factors that influence cation inversion between tetrahedral and octahedral sites are the nature and combination of the cations, the cation radii and charge, the electrostatic contribution to the lattice energy, and the crystal-field effects. Also, the cation distribution is directly and strongly influenced by the thermal treatment. Recently, Bordeneuve at al. reported a dense ceramic sample of $Co_xMn_{3-x}O_4$ ($x = 0.93$) having only 1% of Co atoms residing on the octahedral site at RT, although samples were quenched to RT from high sintering temperatures (1160−1300 °C) and one could expect that a sudden cooling would preserve a high-temperature distribution characterized with a larger degree of disorder.[52] The electric and magnetic properties of spinel oxides are closely related to the cation arrangements, and therefore a complete crystallographic description of the prepared oxide is considered to be a necessity.

Structural Study of $CoMn_2O_4$. Powder XRD studies revealed that heating of compound **1** at 800 °C led to formation of the $CoMn_2O_4$ phase. A similar composition was found for the product prepared at even lower temperatures by heating **1** at 500 °C, but broad and unresolved diffraction lines indicated very small crystallite sizes at that point. The RT structure of $CoMn_2O_4$ can be described as a spinel, which is tetragonal-distorted because of the Jahn−Teller effect associated with a d^4 high-spin electronic configuration of Mn^{3+}. The structure has been refined from the powder data in the $I4_1/amd$ space group, with the unit cell parameters $a = b = 5.7235(2)$ Å and $c = 9.2695(5)$ Å. The structure $^{tet}[Co^{2+},Mn^{3+}]^{oct}[Mn^{3+},Co^{2+}]_2O_4$, presuming a nonzero inversion parameter ($\delta \neq 0$), was used as the starting structural model. Cations in the tetrahedral and octahedral sites are located on special positions 4a and 8d, respectively; therefore, coordinates were not refined, while the atomic coordinates for an oxygen anion residing on the general position 16h were refined. Isotropic temperature factors were refined for each crystallographic site, not individually for each cation. The inversion parameter was obtained from the refined value of the occupancy parameter to which Co^{2+} and Mn^{3+} cations were constrained with respect to the overall stoichiometry. Reported values converged at the final refinement step. The graphical result of the Rietveld refinement is shown in Figure 7; good agreement of the observed and calculated patterns unambiguously confirms formation of the $CoMn_2O_4$ phase.

The crystal data and a summary of the structure refinement for the oxide $CoMn_2O_4$ are given in Table 3, whereas refined fractional atomic coordinates and thermal parameters are presented in Table S1 in the Supporting Information (SI).

Table 3. Crystal Data and Summary of the Structure Refinement for $CoMn_2O_4$

phase	$CoMn_2O_4$
formula sum	$Co_{4.00}Mn_{8.00}O_{16.00}$
formula mass (g mol^{-1})	931.22
density (calcd) (g cm^{-3})	5.09
space group	$I\,4_1/amd$ (No. 141)
lattice param	
a (Å)	5.7235(2)
c (Å)	9.2695(5)
V ($\times 10^6$ pm^3)	303.65(3)
fitting mode	structure fit
profile function	pseudo-Voigt
U	0.09(3)
V	−0.02(1)
W	0.144(1)
asymmetry parameter 1	0.0043(1)
peak-shape parameter 1	0.58(2)
peak-shape parameter 2	0.009(1)
R(weighted profile) (%)	3.458
R(profile) (%)	2.472
GOF	1.109

From refined structural parameters (Table S1 in the SI), one can see that the phase obtained by the thermal treatment of **1** at 800 °C is characterized by the inversion parameter $\delta = 21\%$, and therefore the structural formula can be written as $^{tet}[Co_{0.79}Mn_{0.21}]^{oct}[Mn_{0.895}Co_{0.105}]_2O_4$. The tetrahedral site 4a is occupied by ∼80% of Co and ∼20% of Mn. The octehadral site 8d is occupied by ∼90% of Mn and ∼10% of Co. The crystal structure is given in Figure 8. Selected interatomic

dx.doi.org/10.1021/ic501134y | Inorg. Chem. 2014, 53, 9633−9643

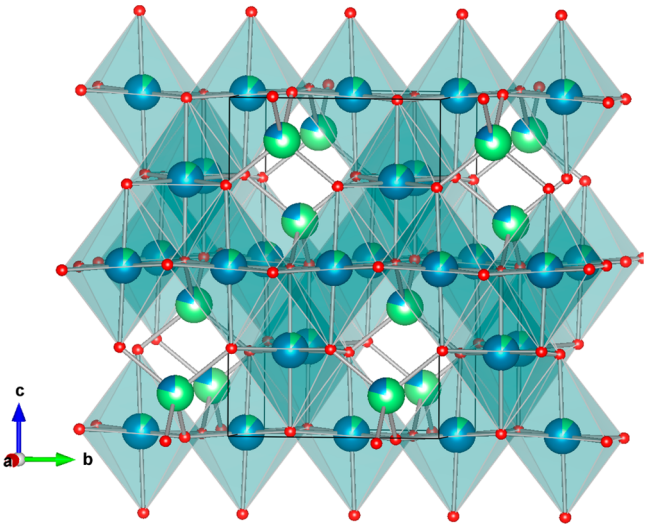

Figure 8. Crystal structure of the $CoMn_2O_4$ phase in the *bc* plane. The tetrahedral site 4a is occupied by ~80% of Co (light green) and ~20% of Mn (blue). The octehadral site 8d is occupied by ~90% of Mn (blue) and ~10% of Co (light green). Octahedra around the 8d site are given as blue-green, while tetrahedra around the 4a site are omitted for clarity.

distances are listed in Table 4. There are two types of M_{oct}–M_{oct} distances between the adjacent octahedral units connected by the edge, two types of M_{oct}–M_{tet} distances between the adjacent octahedra and tetrahedra connected by corners, and one type of M_{tet}–M_{tet} distance between the closest tetrahedral units. The shortest distance between metal centers is found in the chains of M_{oct}–O_6 running parallel to the *a* and *c* axes, and it amounts to 2.8618(1) Å.

Table 4. Selected Bond Distances (Å) in the Structure of $CoMn_2O_4$

M_{tet}–O(×4)	1.967(2)
M_{oct}–O(×4)	1.965(2)
M_{oct}–O(×2)	2.227(3)
M_{oct}–M_{tet}	3.4029(1), 3.759(1)
M_{oct}–M_{oct}	3.0765(9), 2.8618(1)
M_{tet}–M_{tet}	3.6823(1)

Cobalt(II) dimanganate prepared by heat treatment at 800 °C is characterized by an average crystallite size of 310(20) Å, as obtained by size–strain analysis during the Rietveld refinement. Crystallite sizes in two different crystallographic directions were calculated by the *XBroad* program[43] implemented with the Warren–Averbach method.[45] Figure 9 shows an area-weighted size of the coherent diffraction domain in the directions perpendicular to lattice planes (020) and (004). As can be seen, the crystallite dimension in the direction of the *a* axis amounts to 331(12) Å, while the size in the direction of the *c* axis amounts to 303(11) Å, indicating nearly isometric crystallite shape.

IR Study of $CoMn_2O_4$. Generally, the IR spectra of spinel oxides are characterized by absorption bands in the range between 700 and 400 cm^{-1}.[53,54] A relatively strong absorption band corresponding to the stretching vibration of the atom in the tetrahedral oxygen environment [ν(CoO)] is located at 638 cm^{-1} in the spectrum of **1**. The strong band present at 542 cm^{-1} indicates the stretching vibrations of the atom in the octahedral oxygen environment [mainly ν(MnO)]. A medium-intensity absorption band at 420 cm^{-1} could be ascribed to the vibration mode of Co–O–Mn. The broad band of weak intensity with a maximum of around 3447 cm^{-1} is in agreement with the presence of chemisorbed water.[53,54]

Magnetization Study of $CoMn_2O_4$. The temperature dependence of magnetization, $M(T)$, for $CoMn_2O_4$ shown in Figure 10 reveals the development of at least three magnetic phases as the temperature changes from 2 to 360 K. The sharp peak at the ZFC curve for the lowest field (100 Oe in Figure 10) points to antiferromagnetic nature of the transition at 83 K. With an increase of the field, this peak moves slightly to lower temperatures (82 K for 1000 Oe). For a high field of 10 kOe, this peak becomes broad (maximum at 77 K) but still persists. On FC curves, there are marks of this transition, but these are not expressed considerably because of superposition with some unfrozen magnetization, which dominates. Other works mention phase transition at 90 and 70 K.[22,55] The transition at 70 K was studied with neutron diffraction and confirmed the collinear ferrimagnetic structure.[55] Our results also show ferrimagnetic behavior because the FC magnetization value is

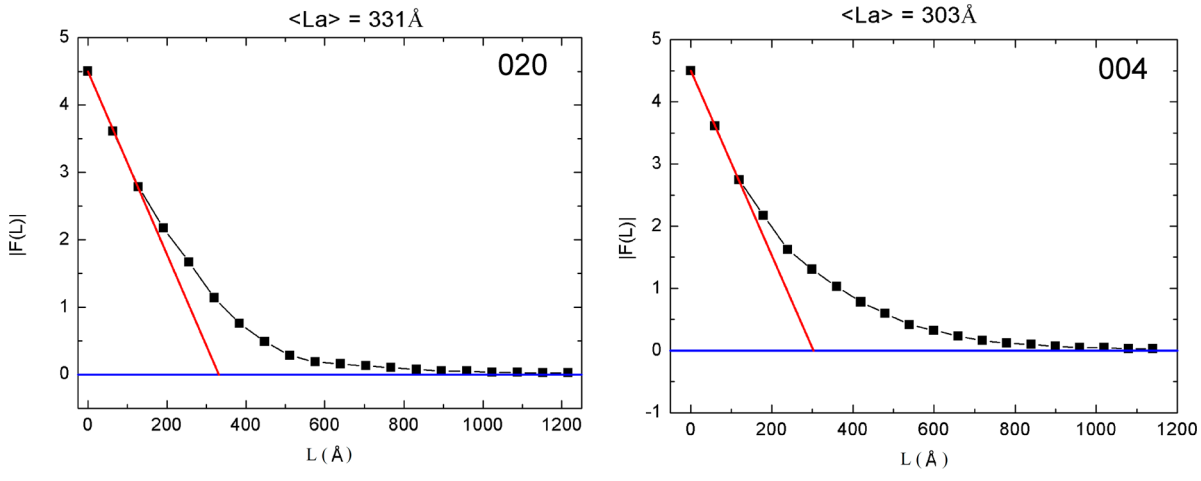

Figure 9. Result of line-broadening analysis of a sample obtained by the heat treatment of **1** at 800 °C. The area-weighted coherent diffraction domain $\langle L_a \rangle$ is calculated in the directions perpendicular to lattice planes (020) and (004), respectively.

dx.doi.org/10.1021/ic501134y | *Inorg. Chem.* 2014, 53, 9633–9643

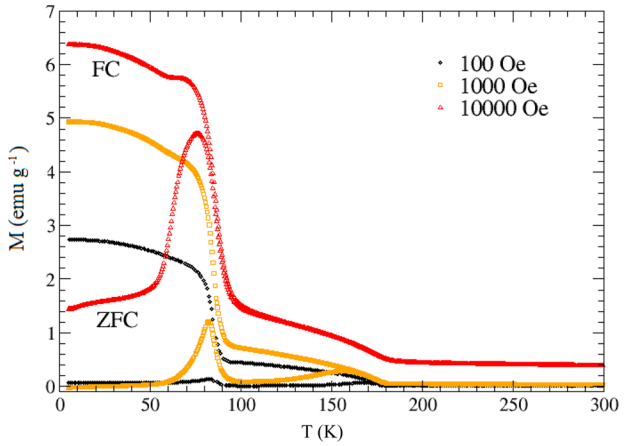

Figure 10. Temperature dependence of magnetization for the oxide $CoMn_2O_4$ for ZFC and FC states.

considerably high, but the transition is at somewhat higher temperature, which may originate from different spinel inversion degrees. At 180 K, there is another magnetic transition characterized with ZFC−FC splitting below and paramagnetic-like behavior above (Figure 10). In order to distinguish the observed transitions, magnetic hysteresis loops were measured at many different temperatures, and some representative curves are shown in Figure 11. At 5 K, there is

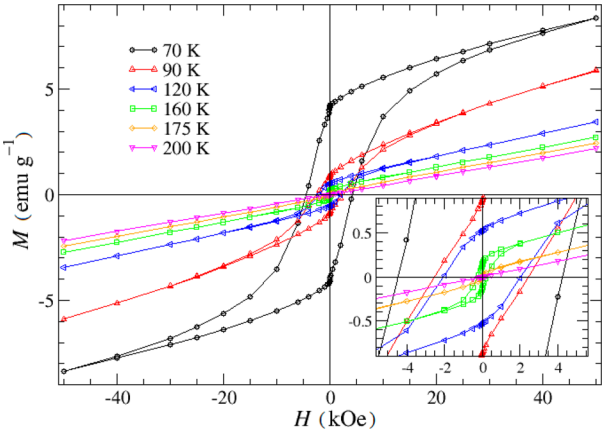

Figure 11. Magnetic hysteresis loops of the oxide $CoMn_2O_4$ at different temperatures. Inset: Enlargement of the small-field region.

unusually large hysteresis with a coercive field of 20 kOe (not shown because it is not closed because the irreversibility field is much larger than the available 50 kOe), and at 70 K, the coercive field is still 4.2 kOe (with an irreversibility field at about 40 kOe).

The paramagnetic state is therefore suggested above 180 K in the sense of linear $M(H)$. However, the $M(T)$ curves cannot be fitted with Curie−Weiss law satisfactorily, and the effective magnetic moment is not possible to extract. Namely, the product χT amounts to 2.1 emu mol^{-1} K at 200 K and 2.7 emu mol^{-1} K at 300 K, which is still at least 3 times less than what is needed for the corresponding Co and Mn ions altogether in the paramagnetic state. This could originate from organization of the spins into multiples behaving as paramagnetic units and/or from the strong influence of spin−orbit coupling in Co^{2+} ions in the spinel lattice, as well as the remaining correlations (also of the antiferromagnetic type) between magnetic moments. Antiferromagnetic interaction is responsible for so low magnetization (being far from saturation) in the highest fields in the low-temperature region also. However, wide hysteresis can originate from the nanoparticulate structure where the net magnetization could come from spin canting and disorder on the surface layer of the nanoparticles.[56,57]

The behavior between 83 and 180 K, intermediate between the already known ferrimagnetic phase (antiferromagnetic-like transition) and a paramagnetic-like phase, is very interesting because it shows the possibility of tuning the hysteresis and ZFC−FC splitting with preparation conditions and morphology. Namely, according to the literature,[22] this region in $M(T)$ is determined with the size of the nanocrystallites. Generally, splitting between the ZFC and FC curves points to the blocking of the magnetic moments of the nanoparticles. Here the observed shift of splitting between the ZFC and FC curves toward lower temperatures with an increase of the field is in agreement with the influence of the magnetic field upon lowering of the barriers (Figure 10).[58] On the other hand, hysteresis having shape reminiscent of magnetic nanoparticles becomes narrower as the temperature increases, showing that reorientation of the moments becomes easier with smaller field due to higher thermal energy. This blocking of the magnetic moments was suppressed to temperatures below 80 K (therefore, unobservable because of superposition with additional ferrimagnetic transitions) for nanoparticles smaller than 20 nm[31b] and was observable only for 45 nm and bigger.[22] Therefore, the behavior of our oxide with an average crystallite size of 31 nm is in accordance with the already observed superparamagnetism of the nanocrystallites in similar $CoMn_2O_4$ structures. Moreover, our results set up the new boundary for blocking of the superparamagnetic moments: our crystallites/particles of 31 nm size still exhibit the blocking up to 180 K in small applied magnetic fields (whereas previous studies did not consider particles between 20 and 45 nm[22,31b]).

Summarizing the magnetic results for $CoMn_2O_4$, we can conclude that the ferrimagnetic state is observed below 83 K, and up to 180 K blocking of the magnetic moments of nanocrystallites appears, transforming to nontrivial paramagnetic-like behavior above 180 K.

CONCLUSIONS

A one-step synthetic route for the preparation of the $CoMn_2O_4$ spinel has been established, using 3D heterobimetallic oxalate-bridged compound **1** via thermal decomposition. This coordination polymer shows magnetic ordering below 13 K and has proved to be a good single-source precursor because of its simple synthesis, without usage of organic solvents but mostly of water. Our magnetic measurement results for $CoMn_2O_4$, obtained by a SQUID magnetometer, indicate blocking of the superparamagnetic moments: our crystallites of 31 nm size still exhibit blocking up to 180 K in small applied magnetic fields (whereas previous studies did not consider particles between 20 and 45 nm). Microstructural characterization of the $CoMn_2O_4$ sample was carried out by the means of XRD line-broadening analysis, explaining the observed change of the properties. This opens a new possibility for tuning the spinel properties dependent on the size and morphology of nanocrystals, like enhanced blocking of magnetization and increased coercivity, as well as other phenomena useful in the application for sensing and catalysis.

The investigation of other important properties of the nanophase $CoMn_2O_4$ oxide prepared from molecular precursor

dx.doi.org/10.1021/ic501134y | Inorg. Chem. 2014, 53, 9633−9643

1, such as the crystallite size depending on the heating temperature, is currently underway. The electric and magnetic properties of spinel oxides are closely related to the cation arrangements, whose distribution is directly and strongly influenced by the thermal treatment.

Our further research would be related to the synthesis and characterization of similar 3D oxalate complexes [with different tris(oxalato)metalate anions, $[M(C_2O_4)_3]^{3-}$, and/or tris-chelated cations, $[M(bpy)_3]^{2+}$ or $[M(bpy)_3]^{3+}$] and their molecular precursor-to-material conversion to the mixed-metal oxides.

■ ASSOCIATED CONTENT

Supporting Information

Atomic coordinates for $CoMn_2O_4$ (Table S1) and X-ray crystallographic files (CIFs) for compound **1** and the oxide $CoMn_2O_4$. This material is available free of charge via the Internet at http://pubs.acs.org.

■ AUTHOR INFORMATION

Corresponding Author

*E-mail: Marijana.Juric@irb.hr. Tel.: +385 1 4561-189. Fax: +385 1 4680-098.

Notes

The authors declare no competing financial interest.

■ ACKNOWLEDGMENTS

This research was supported by the Ministry of Science, Education and Sports of the Republic of Croatia (Grants 098-0982904-2946, 098-1191344-2943, and 119-1191458-1017). The authors are grateful to Dr. Željko Skoko for recording the powder XRD patterns.

■ REFERENCES

(1) Kuppler, R. J.; Timmons, D. J.; Fang, Q.-R.; Li, J.-R.; Makal, T. A.; Young, M. D.; Yuan, D.; Zhao, D.; Zhuang, W.; Zhou, H.-C. *Coord. Chem. Rev.* **2009**, *253*, 3042−3066.

(2) Suh, M. P.; Cheon, Y. E.; Lee, E. Y. *Coord. Chem. Rev.* **2008**, *252*, 1007−1026.

(3) James, S. L. *Chem. Soc. Rev.* **2003**, *32*, 276−288.

(4) Allen, F. H. *Acta Crystallogr.* **2002**, *B58*, 380−388.

(5) (a) Zhong, Z. J.; Matsumoto, N.; Ōkawa, H.; Kida, S. *Chem. Lett.* **1990**, 87−90. (b) Tamaki, H.; Zhong, Z. J.; Matsumoto, N.; Kida, S.; Koikawa, M.; Achiwa, N.; Hashimoto, Y.; Ōkawa, H. *J. Am. Chem. Soc.* **1992**, *114*, 6974−6979. (c) Atovmyan, L. O.; Shilov, G. V.; Lyubovskaya, R. N.; Zhilyaeva, E. I.; Ovanesyan, N. S.; Pirumova, S. I.; Gusakovskaya, I. G.; Morozov, Y. G. *JETP Lett.* **1993**, *58*, 766−769.

(6) (a) Decurtins, S.; Schmalle, H. W.; Oswald, H. R.; Linden, A.; Ensling, J.; Gütlich, P.; Hauser, A. *Inorg. Chim. Acta* **1994**, *216*, 65−73. (b) Farrell, R. P.; Hambley, T. W.; Lay, P. A. *Inorg. Chem.* **1995**, *34*, 757−758. (c) Pellaux, R.; Schmalle, H. W.; Huber, R.; Fischer, P.; Hauss, T.; Ouladdiaf, B.; Decurtins, S. *Inorg. Chem.* **1997**, *36*, 2301−2308.

(7) (a) Carling, S. G.; Mathonière, C.; Day, P.; Malik, K. M. A.; Coles, S. J.; Hursthouse, M. B. *J. Chem. Soc., Dalton Trans.* **1996**, 1839−1843. (b) Mathonière, C.; Nuttall, C. J.; Carling, S. G.; Day, P. *Inorg. Chem.* **1996**, *35*, 1201−1206. (c) Watts, I. D.; Carling, S. G.; Day, P. *J. Chem. Soc., Dalton Trans.* **2002**, 1429−1434.

(8) (a) Larionova, J.; Mombelli, B.; Sanchiz, J.; Kahn, O. *Inorg. Chem.* **1998**, *37*, 679−684. (b) Andrés, R.; Gruselle, M.; Malézieux, B.; Verdaguer, M.; Vaissermann, J. *Inorg. Chem.* **1999**, *38*, 4637−4646.

(9) (a) Bénard, S.; Yu, P.; Audière, J. P.; Rivière, E.; Clément, R.; Guilhem, J.; Tchertanov, L.; Nakatani, K. *J. Am. Chem. Soc.* **2000**, *122*, 9444−9454. (b) Evans, J. S. O.; Bénard, S.; Yu, P.; Clement, R. *Chem. Mater.* **2001**, *13*, 3813−3816.

(10) Malézieux, B.; Andrés, R.; Brissard, M.; Gruselle, M.; Train, C.; Herson, P.; Troitskaya, L. L.; Sokolov, V. I.; Ovseenko, S. T.; Demeschik, T. V.; Ovanesyan, N. S.; Mamed'yarova, I. A. *J. Organomet. Chem.* **2001**, *637*−*639*, 182−190.

(11) (a) Clemente-León, M.; Coronado, E.; Galán-Mascarós, J.-R.; Gómez-García, C. J. *Chem. Commun.* **1997**, 1727−1728. (b) Coronado, E.; Galán-Mascarós, J.-R.; Gómez-García, C. J.; Martínez-Agudo, J. M. *Adv. Mater.* **1999**, *11*, 558−561. (c) Coronado, E.; Galán-Mascarós, J.-R.; Gómez-García, C. J.; Laukhin, V. *Nature* **2000**, *408*, 447−449. (d) Coronado, E.; Galán-Mascarós, J.-R.; Gómez-García, C. J.; Ensling, J.; Gutlich, P. *Chem.—Eur. J.* **2000**, *6*, 552−563. (e) Coronado, E.; Galán-Mascarós, J.-R.; Gómez-García, C. J.; Martínez-Agudo, J. M. *Inorg. Chem.* **2001**, *40*, 113−120.

(12) (a) Decurtins, S.; Schmalle, H. W.; Schneuwly, P.; Oswald, H. R. *Inorg. Chem.* **1993**, *32*, 1888−1892. (b) Decurtins, S.; Schmalle, H. W.; Schneuwly, P.; Ensling, J.; Gütlich, P. *J. Am. Chem. Soc.* **1994**, *116*, 9521−9528. (c) Pointillart, F.; Train, C.; Gruselle, M.; Villain, F.; Schmalle, H. W.; Talbot, D.; Gredin, P.; Decurtins, S.; Verdaguer, M. *Chem. Mater.* **2004**, *16*, 832−841. (d) Pointillart, F.; Train, C.; Boubekeur, K.; Gruselle, M.; Verdaguer, M. *Tetrahedron: Asymmetry* **2006**, *17*, 1937−1943. (e) Li, Y.; Zhang, Z.-X.; Li, K.-C.; Song, W.-D.; Li, Q.-S. *Inorg. Chem. Commun.* **2007**, *10*, 1557−1560.

(13) (a) Hernández-Molina, M.; Lloret, F.; Ruiz-Pérez, C.; Julve, M. *Inorg. Chem.* **1998**, *37*, 4131−4135. (b) Decurtins, S.; Schmalle, H. W.; Pellaux, R.; Schneuwly, P.; Hauser, A. *Inorg. Chem.* **1996**, *35*, 1451−1460.

(14) (a) Román, P.; Guzmán-Miralles, C.; Luque, A. *J. Chem. Soc., Dalton Trans.* **1996**, 3985−3989. (b) Pellaux, R.; Decurtins, S.; Schmalle, H. W. *Acta Crystallogr.* **1999**, *C55*, 1075−1079. (c) Sieber, R.; Decurtins, S.; Stoeckli-Evans, H.; Wilson, C.; Yufit, D.; Howard, J. A. K.; Capelli, S. C.; Hauser, A. *Chem.—Eur. J.* **2000**, *6*, 361−368.

(15) (a) Andrés, R.; Brissard, M.; Gruselle, M.; Train, C.; Vaissermann, J.; Malézieux, B.; Jamet, J.-P.; Verdaguer, M. *Inorg. Chem.* **2001**, *40*, 4633−4640. (b) Clemente-León, M.; Coronado, E.; Gómez-García, C. J.; Soriano-Portillo, A. *Inorg. Chem.* **2006**, *45*, 5653−5660. (c) Clemente-León, M.; Coronado, E.; López-Jordà, M.; Waerenborgh, J. C. *Inorg. Chem.* **2011**, *50*, 9122−9130. (d) Pardo, E.; Train, C.; Liu, H.; Chamoreau, L.-M.; Dkhil, B.; Boubekeur, K.; Lloret, F.; Nakatani, K.; Tokoro, H.; Ohkoshi, S.-i.; Verdaguer, M. *Angew. Chem., Int. Ed.* **2012**, *5*, 8356−8360. (e) Clemente-León, M.; Coronado, E.; Gómez-García, C. J.; López-Jordà, M.; Camón, A.; Repollés, A.; Luis, F. *Chem.—Eur. J.* **2014**, *20*, 1669−1676.

(16) (a) Clemente-León, M.; Coronado, E.; Giménez-López, M. C.; Soriano-Portillo, A.; Waerenborgh, J. C.; Delgado, F. S.; Ruiz-Pérez, C. *Inorg. Chem.* **2008**, *47*, 9111−9120. (b) Clemente-León, M.; Coronado, E.; López-Jordà, M.; Waerenborgh, J. C. *Inorg. Chem.* **2011**, *50*, 9122−9130. (c) Pardo, E.; Train, C. T.; Gontard, G.; Boubekeur, K.; Fabelo, O.; Liu, H.; Dkhil, B.; Lloret, F.; Nakagawa, K.; Tokoro, H.; Ohkoshi, S.-i.; Verdaguer, M. *J. Am. Chem. Soc.* **2011**, *133*, 15328−15331. (d) Clemente-León, M.; Coronado, E.; López-Jordà, M.; Desplanches, C.; Asthana, S.; Wang, H.; Létard, J.-F. *Chem. Sci.* **2011**, *2*, 1121−1127. (e) Clemente-León, M.; Coronado, E.; Martí-Gastaldo, C.; Romero, F. M. *Chem. Soc. Rev.* **2011**, *40*, 473−497. (f) Clemente-León, M.; Coronado, E.; López-Jordà, M. *Dalton Trans.* **2013**, *42*, 5100−5110. (g) Clemente-León, M.; Coronado, E.; López-Jordà, M.; Waerenborgh, J. C.; Desplanches, C.; Wang, H.; Létard, J.-F.; Hauser, A.; Tissot, A. *J. Am. Chem. Soc.* **2013**, *135*, 8655−8667.

(17) (a) Coronado, E.; Galán-Mascarós, J. R.; Martí-Gastaldo, C. *J. Am. Chem. Soc.* **2008**, *130*, 14987−14989. (b) Pardo, E.; Train, C.; Boubekeur, K.; Gontard, G.; Cano, J.; Lloret, F.; Nakatani, K.; Verdaguer, M. *Inorg. Chem.* **2012**, *51*, 11582−11593.

(18) Nunes, G. G.; Seisenbaeva, G. A.; Kessler, V. G. *Cryst. Growth. Des.* **2011**, *11*, 1238−1243.

(19) Bayot, D.; Tinant, B.; Devillers, M. *Inorg. Chem.* **2005**, *44*, 1554−1562.

(20) Thurston, J. H.; Whitmire, K. H. *Inorg. Chem.* **2003**, *42*, 2014−2023.

(21) Thurston, J. H.; Whitmire, K. H. *Inorg. Chem.* **2002**, *41*, 4194−4205.

(22) Mahata, P.; Sarma, D.; Madhu, C.; Sundaresen, A.; Natarajan, S. *Dalton Trans.* **2011**, *40*, 1952−1960.
(23) Neo, K. E.; Ong, Y. Y.; Huynh, H. V.; Hor, T. S. A. *J. Mater. Chem.* **2007**, *17*, 1002−1006.
(24) Guo, L.; Arafune, H.; Teramae, N. *Langmuir* **2013**, *29*, 4404−4412.
(25) Rhine, W. E.; Hallock, R. B.; Davis, W. M.; Wong-Ng, W. *Chem. Mater.* **1992**, *4*, 1208−1216.
(26) Wada, S.; Narahara, M.; Hoshina, T.; Kakemoto, H.; Tsurumi, T. *J. Mater. Sci.* **2003**, *38*, 2655−2660.
(27) Androš, L.; Matković-Čalogović, D.; Planinić, P. *CrystEngComm* **2013**, *15*, 533−543.
(28) Jurić, M.; Planinić, P.; Brničević, N.; Matković-Čalogović, D. *J. Mol. Struct.* **2008**, *888*, 266−276.
(29) (a) Jurić, M.; Popović, J.; Šantić, A.; Molčanov, K.; Brničević, N.; Planinić, P. *Inorg. Chem.* **2013**, *52*, 1832−1842. (b) Popović, J.; Vrankić, M.; Jurić, M. *Cryst. Growth Des.* **2013**, *13*, 2161−2165.
(30) Androš, L.; Jurić, M.; Popović, J.; Šantić, A.; Lazić, P.; Benčina, M.; Valant, M.; Brničević, N.; Planinić, P. *Inorg. Chem.* **2013**, *52*, 14299−14308.
(31) (a) Cheng, F.; Shen, J.; Peng, B.; Pan, Y.; Tao, Z.; Chen, J. *Nat. Chem.* **2011**, *3*, 79−84. (b) Zhang, H. T.; Chen, X. H. *Nanotechnology* **2006**, *171*, 1384−1390.
(32) Coronado, E.; Martí-Gastaldo, C.; Galán-Mascarós, J. R.; Cavallini, M. *J. Am. Chem. Soc.* **2010**, *132*, 5456−5468.
(33) (a) Liu, J.; Li, F.; Evans, D. G.; Duan, X. *Chem. Commun.* **2003**, 542−543. (b) Li, F.; Liu, J.; Evans, D. G.; Duan, X. *Chem. Mater.* **2004**, *16*, 1597−1602. (c) Kobayashi, Y.; Ke, X.; Hata, H.; Schiffer, P.; Mallouk, T. E. *Chem. Mater.* **2008**, *20*, 2374−2381.
(34) (a) Manova, E.; Kunev, B.; Paneva, D.; Mitov, I.; Petrov, L.; Estournès, C.; D'Orléans, C.; Rehspringer, J.-L.; Kurmoo, M. *Chem. Mater.* **2004**, *16*, 5689−5696. (b) Manova, E.; Paneva, D.; Kunev, B.; Estournès, Cl.; Rivière, E.; Tenchev, K.; Léaustic, A.; Mitov, I. *J. Alloys Compd.* **2009**, *485*, 356−361. (c) Manova, E.; Tsoncheva, T.; Paneva, D.; Popova, M.; Velinov, N.; Kunev, B.; Tenchev, K.; Mitov, I. *J. Solid State Chem.* **2011**, *184*, 1153−1158.
(35) Cartledge, G. H.; Ericks, W. P. *J. Am. Chem. Soc.* **1936**, *58*, 2061−2065.
(36) Jaeger, F. M.; van Dijk, J. A. *Z. Anorg. Allg. Chem.* **1936**, *227*, 273−327.
(37) *CrysAlisPRO*; Oxford Diffraction Ltd.: Oxford, U.K., 2007.
(38) Farrugia, L. J. *J. Appl. Crystallogr.* **1999**, *32*, 837−838.
(39) Sheldrick, G. M. *Acta Crystallogr.* **2008**, *A24*, 112−122.
(40) Spek, A. L. *J. Appl. Crystallogr.* **2003**, *36*, 7−13.
(41) Farrugia, L. J. *J. Appl. Crystallogr.* **1997**, *30*, 568.
(42) Macrae, C. F.; Edgington, P. R.; McCabe, P.; Pidcock, E.; Shields, G. P.; Taylor, R.; Towler, M.; van de Streek, J. *J. Appl. Crystallogr.* **2006**, *39*, 453−457.
(43) Skoko, Ž.; Popović, J.; Dekanić, K.; Kolbas, V.; Popović, S. *J. Appl. Crystallogr.* **2012**, *45*, 594−597.
(44) Stokes, A. R. *Proc. Phys. Soc. London* **1948**, *61*, 382−391.
(45) Warren, B. E. *X-ray Diffraction*; Addison-Wesley: New York, 1969.
(46) Momma, K.; Izumi, F. *J. Appl. Crystallogr.* **2011**, *44*, 1272−1276.
(47) Cartledge, G. H.; Ericks, W. P. *J. Am. Chem. Soc.* **1936**, *58*, 2061−2065.
(48) Nakamoto, K. *Infrared and Raman Spectra of Inorganic and Coordination Compounds*, 6th ed.; John Wiley: New York, 2009.
(49) Boča, R.; Dlháň, L.; Linert, W.; Ehrenberg, H.; Fuess, H.; Haase, W. *Chem. Phys. Lett.* **1999**, *307*, 359−366.
(50) Kahn, O. *Molecular Magnetism*; Wiley-VCH: New York, 1993; pp 31−43.
(51) Figgis, B. N.; Gerloch, M.; Lewis, J.; Mabbs, F. E.; Webb, G. A. *J. Chem. Soc. A* **1968**, 2086−2093.
(52) Bordeneuve, H.; Tenailleau, C.; Guillemet-Fritsch, S.; Smith, R.; Suard, E.; Rousset, A. *Solid State Sci.* **2010**, *12*, 379−386.
(53) Hosseini, S. A.; Niaei, A.; Salari, D.; Nabavi, S. R. *Ceram. Int.* **2012**, *38*, 1655−1661.
(54) Salker, A. V.; Gurav, S. M. *J. Mater. Sci.* **2000**, *35*, 4713−4719.
(55) Boucher, B.; Buhl, R.; Perrin, M. *J. Appl. Phys.* **1968**, *39*, 632.
(56) Zysler, R. D.; Winkler, E.; Vasquez Mansilla, M.; Fiorani, D. *Physica B* **2006**, *384*, 277−281.
(57) Parker, F. T.; Foster, M. W.; Margulies, D. T.; Berkowitz, A. E. *Phys. Rev. B* **1993**, *47*, 7885−7891.
(58) Pajić, D.; Zadro, K.; Ristić, R.; Živković, I.; Skoko, Ž.; Babić, E. *J. Phys.: Condens. Matter* **2007**, *19*, 296207.